

THE 3RD IBIS/ISGRI SOFT GAMMA-RAY SURVEY CATALOG *

A. J. BIRD^A, A. MALIZIA^B, A. BAZZANO^C, E. J. BARLOW^A, L. BASSANI^B, A. B. HILL^A, G. BÉLANGER^D, F. CAPITANIO^{A,C}, D. J. CLARK^A, A. J. DEAN^A, M. FIOCCHI^C, D. GÖTZ^D, F. LEBRUN^D, M. MOLINA^A, N. PRODUIT^{F,G}, M. RENAUD^D, V. SGUERA^A, J. B. STEPHEN^B, R. TERRIER^E, P. UBERTINI^C, R. WALTER^{F,G}, C. WINKLER^H, J. ZURITA^D

Draft version June 12, 2021

ABSTRACT

In this paper we report on the third soft gamma-ray source catalog obtained with the IBIS/ISGRI gamma-ray imager on board the INTEGRAL satellite. The scientific dataset is based on more than 40 Ms of high quality observations performed during the first three and a half years of Core Programme and public IBIS/ISGRI observations. Compared to previous IBIS/ISGRI surveys, this catalog includes a substantially increased coverage of extragalactic fields, and comprises more than 400 high-energy sources detected in the energy range 17–100 keV, including both transients and faint persistent objects which can only be revealed with longer exposure times.

Subject headings: gamma-rays: observations, surveys, Galaxy:general

1. INTRODUCTION

Since its launch in 2002, the INTEGRAL (International Gamma-Ray Astrophysics Laboratory) observatory has carried out more than 4 years of observations in the energy range from 5 keV – 10 MeV. INTEGRAL is an observatory-type mission, and most of the total observing time (65% in the nominal phase, 75% during the mission extension) is awarded as the General Programme to the scientific community at large. Typical observations last from 100 ks up to two weeks. As a return to the international scientific collaborations and individual scientists who contributed to the development, design and procurement of INTEGRAL, a part of the observing time (from 35% to 25%) is allocated to the Core Programme. During the nominal lifetime, this programme consisted of three elements, a deep exposure of the Galactic central radian, regular scans of the Galactic Plane, pointed observations of the Vela region and Target of Opportunity follow-ups (Winkler 2003).

The IBIS (Imager on Board INTEGRAL spacecraft) imaging instrument is optimised for survey work with a large (30°) field of view with excellent imaging and spectroscopy capability (Ubertini et al. 2003), and has formed the basis of several previous INTEGRAL surveys.

*BASED ON OBSERVATIONS WITH INTEGRAL, AN ESA PROJECT WITH INSTRUMENTS AND SCIENCE DATA CENTRE FUNDED BY ESA MEMBER STATES (ESPECIALLY THE PI COUNTRIES: DENMARK, FRANCE, GERMANY, ITALY, SWITZERLAND, SPAIN), CZECH REPUBLIC AND POLAND, AND WITH THE PARTICIPATION OF RUSSIA AND THE USA.

^a School of Physics and Astronomy, University of Southampton, SO17 1BJ, UK

^b IASF-INAF, Via Gobetti 101, 40129 Bologna, Italy

^c IASF-INAF, Via Fosso del Cavaliere 100, 00133 Rome, Italy

^d CEA-Saclay, DAPNIA/Service d’Astrophysique, F91191, Gif sur Yvette Cedex, France

^e Federation de recherche APC, College de France 11, place Marcelin Berthelot, F75231, Paris, France

^f Geneva Observatory, University of Geneva, Chemin des Maillettes 51, CH–1290 Sauverny, Switzerland

^g INTEGRAL Science Data Centre, Chemin d’Ecogia 16, CH–1290 Versoix, Switzerland

^h ESA-ESTEC, Research and Scientific Support Dept., Keplerlaan 1, 2201 AZ, Noordwijk, The Netherlands

The frequent Galactic Plane Scans (GPS) within the Core Programme, performed in the first year of operations, were successfully exploited to yield a first survey of the galactic plane to a depth of ~ 1 mCrab in the central radian (Bird et al. 2004). This gave evidence of a soft gamma-ray sky populated with more than 120 sources, including a substantial fraction of previously unseen sources. The second IBIS/ISGRI catalog (Bird et al. 2006) used a greatly increased dataset (of ~ 10 Ms) to unveil a soft gamma-ray sky comprising 209 sources, again with a substantial component ($\sim 25\%$) of new and unidentified sources.

2. THE IBIS ‘ALL SKY’ SURVEY

In this paper we provide the third IBIS/ISGRI soft gamma-ray survey catalog, comprising more than 400 high-energy sources.

The instrumental details and sensitivity can be found in Lebrun et al. (2003) and Ubertini et al. (2003). The data are collected with the low-energy array, ISGRI (INTEGRAL Soft Gamma-Ray Imager; Lebrun et al. (2003)), consisting of a pixellated 128x128 CdTe solid-state detector that views the sky through a coded aperture mask. IBIS/ISGRI generates images of the sky with a 12’ (FWHM) resolution and arcmin source location accuracy over a $\sim 19^\circ$ (FWHM) field of view in the energy range 15–1000 keV.

This ‘all sky’ catalog uses mosaic image data from the first 3.5 years of IBIS/ISGRI Core Programme and public observations. The dataset used in this catalog ensures that $>70\%$ of the sky is now observed with an exposure of at least 10ks (see Figure 1). As for previous catalogs, the aim is to provide a prompt release of information to the community.

3. DATA ANALYSIS AND CATALOG CONSTRUCTION

The methods used for production of this catalog are the same as, or close derivatives of, those used in the second IBIS/ISGRI catalog production (Bird et al. 2006). Refinements have been made in various areas, and some techniques have been extended to deal with the larger dataset now in use.

INTEGRAL/IBIS data is organised in short pointings

referred to as science windows (scw) each of typically 2000s. During the majority of observations, the INTEGRAL telescope axis is dithered around the nominal pointing direction by a few degrees in order to aid image reconstruction. In this observing mode, science windows contain data taken either during the pointings or during the short slews between the dither positions; pointing and slew data is not mixed within a science window. A small fraction of the observations are performed in ‘staring’ mode, where the telescope axis is kept fixed on a target for long periods without dithering. In this case, the long pointing is divided into several science windows, but no slews are present.

3.1. Input dataset and pipeline processing

The survey input dataset consists of all pointing data available at the end of May 2006, from revolutions (orbits) 12-429 inclusive, covering the time period from launch to the end of April 2006. This results in more than 40 Ms exposure time in this iteration of the survey analysis.

Pipeline processing was carried out using the latest version of the standard INTEGRAL analysis software (OSA 5.1; Goldwurm et al. (2003)) up to the production of sky images for individual science windows. Five primary search bands (17–30, 18–60, 20–40, 30–60 and 40–100 keV) were used to both optimise the source search sensitivity and provide compatibility with previous datasets. The new version of the OSA software allowed lower energy thresholds to be used than in previous catalogs, improving the sensitivity to sources with very soft spectra.

A catalog of known or expected sources is a key input for the image deconvolution process. The final input catalog used in the image processing described here comprised ~ 350 excesses produced primarily by a preliminary processing of a smaller dataset using *OSA 5.1* and an input catalog based on the second IBIS/ISGRI survey, plus all other INTEGRAL-detected sources (i.e. those with an IGR designation) published up to the start of processing.

3.2. Science window selection

When constructing a final mosaic of all images, it is important to remove the small fraction of images for which the image deconvolution process has not been successful. These mainly include data taken during or following severe solar activity or near spacecraft perigee passages when the background modelling is difficult.

As for the second IBIS/ISGRI catalog production, the image rms (after removal of sources) was used as the primary indicator of image quality. The image rms was determined for each significance map (at science window level), and the distribution of the image rms statistics for all science windows was determined. The mean and variance of this distribution was determined in order to define what can be considered a ‘good’ image rms. An acceptance threshold was then set at 2 sigma above the mean image rms, and any individual images with higher rms than this were discarded. Typically, this resulted in any image with an rms greater than 1.08 (after removal of sources) being rejected. Of the ~ 24000 scw processed, ~ 20000 scw were retained in the final scw list.

Additionally, science windows acquired in ‘staring’ mode, and data taken during the instrument Perfor-

mance Verification (PV) phase (for simplicity, this was taken as up to and including the calibration activities in revolution 45) were removed from the main science window lists due to their potential adverse effect on final mosaic quality. Separate science window lists for staring data and PV data were constructed with higher rms limits to allow for the poorer image quality.

3.3. Mosaic construction

The selected science windows were mosaiced using a proprietary tool optimised to create all-sky galactic maps based on several thousand input science windows.

The higher exposure and long timebase spanned by this latest dataset has introduced a new problem since the second catalog. The source search methods we employ are optimised for detection of persistent flux from a source; a highly variable source may be clearly detectable during outburst, while having an undetectably low mean flux over the full dataset. In order to compensate for this problem, for this third catalog, we constructed mosaics over three timescales. Maps were created for each *revolution* which contained valid data. This is optimised to detect sources active on timescales of the order of a day. We identified 26 sequences of consecutive revolutions which had similar pointings. Thus these *revolution sequences* could best be analysed as a single observation, and sensitivity for sources on longer timescales than revolutions (i.e. order of weeks) could be optimised. Ultimately, persistent sources can best be detected in an *all-archive* accumulation of all available high-quality data.

Maps were created for each of these timescales, in each of the five energy bands described in section 3.1, these being chosen to provide both coverage of the most sensitive energy range for ISGRI and sensitivity to various typical source emission profiles.

For each energy band and time period all-sky mosaics were made in four projections: centred on galactic centre, centred on galactic anti-centre, north galactic polar and south galactic polar. The purpose of these multiple projections is to present the automatic source detection algorithms with source PSFs with the minimum possible distortions.

Additionally, maps were made of the two special datasets: the *staring mode data*, which was excluded from the main mosaics due to the presence of stronger image artefacts which impede the source search algorithms; the *performance verification (PV) data*, which has poorer image quality and would have been largely rejected by the standard rms filters, but contains significant exposure on parts of the sky otherwise poorly exposed. The exposure maps for these three separate datasets are shown in Figure 1.

In total ~ 750 maps were created and searched. Each mosaic used a pixel size of 0.04° ($2.4'$) at the centre of the mosaic in order to optimise source detection and location over the whole mosaic.

3.4. Source searching and location

Each of the mosaics was searched using the *SExtractor 2.4.4* software (Bertin & Arnouts 1996). The source positions measured by *SExtractor* represent the centroid of the source calculated by taking the first order moments of the source profile (referred to by *SExtractor* as the barycenter method).

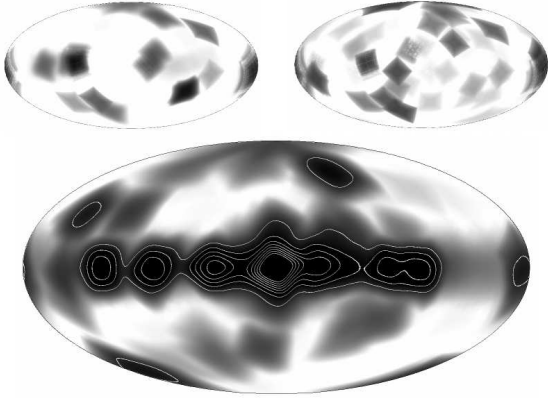


FIG. 1.— Exposure maps for the third IBIS/ISGRI catalog observations: (lower) the all-archive mosaic (contour levels are at 500 ksec) which excludes (top left) performance verification phase exposure and (top right) staring mode data

Source detectability is limited at the faintest levels by background noise and can be improved by the application of a linear filtering of the data. In addition, source confusion in crowded fields can be minimised by the application of a bandpass filter, specifically the *mexhat* bandpass filter is used in the *SExtractor* software. The convolution of the filter with the mosaic alters the source significances, hence *SExtractor* uses the source positions identified from the filtered mosaic to extract the source significances from the original mosaic.

Additional manual checks were performed on each map to check for the (rare) occasions where *SExtractor* fails due to the close proximity of two sources.

3.5. Source list filtering

An initial list of 815 excesses was generated by integration of all lists derived from mosaic images on whole-archive, revolution sequence and revolution timescales.

In order to identify an excess as a source it is necessary first to identify the significance level at which the source population dominates over the noise distribution. To this end we produce a log-log plot of the number of excesses detected by *SExtractor* above a specific significance as a function of that significance. This is shown in Figure 2 for the 30-60 keV all-sky mosaic.

This distribution is fitted by an integrated Gaussian and power law function; the power law component represents the underlying source population and the integrated Gaussian fits to the noise component of the distribution. This model and its components are illustrated in Figure 2: the dashed line represents the power-law component; the dotted line represents the integrated Gaussian component; the dotted-dashed line represents the overall model. Based upon the parameters of the fitted model it is possible to calculate the significance at which the noise distribution contributes 1% of the detected excesses - in the case of the 30-60 keV band mosaic this level is 4.8σ .

However, this cut-off is based upon the global properties of an individual mosaic and the maps contains systematic errors that are not uniformly spatially distributed. The majority of the systematic noise is attributable to the very brightest sources and crowded regions where the deconvolution software has problems

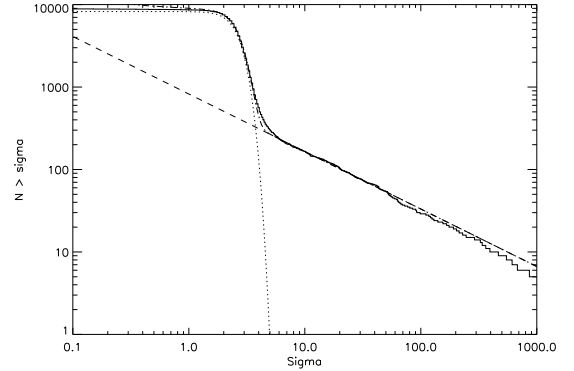


FIG. 2.— Distribution of significances of source-like excesses found in the 30-60 keV all-sky mosaic. The solid line represents the data; the other lines indicate the fit model components, see text for details.

cleaning all of the image artefacts. Consequently the systematic noise is localised to specific regions of the map. In areas with large amounts of systematic noise, such as the Galactic Centre, the cut-off significance will be higher than the global value, while those areas where there is no noticeable systematic noise, principally the extragalactic sky, a lower threshold is appropriate.

The situation is further complicated because each map, with a different energy band, exposure and instrument configuration, will have a subtly different statistical and systematic noise distribution, and hence source detection criteria.

We have applied an initial absolute threshold of 4.5σ in the maps, and all excesses above this threshold were then combined into a preliminary source list. Thereafter, each candidate source was visually inspected and checked for appropriate PSF shape, and removal of systematic map artefacts. When necessary, proprietary tools were used to compare the peaks found in the maps against local rms levels, and perform 2-dimensional gaussian fitting to the source PSFs. Both techniques have been found to aid source extraction in regions of non-statistical background.

After all selection processes, we obtain a source list containing 421 sources, as shown in Table 1 which have been located in the short and long timescale maps.

We can estimate the number of possible false detections in our source list as follows. The analysis for the all-archive map shown in Figure 2 indicates that above 5 sigma significance, there remains a 1% probability of a false detection, while for the revolution and revolution sequence maps, the corresponding figure is 6 sigma. In total, 372 of our sources meet one or both of these criteria and hence we estimate 4 false detections from this sample. The remaining 49 sources should be treated with more caution, and we estimate that 10–20% of these sources may be false detections, noting in passing that our source inspection processes have already discarded 75% of the excesses found between 4.5 and 5 sigma. Hence, overall, we expect that $< 3\%$ of the catalog sources result from false detections, and the majority of these will be sources below 5 sigma (or 6 sigma in the revolution maps).

A number of deep studies have been performed on

the $\sim 4^\circ \times 1^\circ$ region surrounding the Galactic Centre, which is a highly variable sky region containing a group of sources which cannot be de-blended by the imaging capabilities of IBIS alone. For example, Bélanger et al. (2006) provides a study of the Galactic Centre region using both spectral and temporal analyses which are beyond the scope of this broader survey.

4. NOTES ON THE TABLE

4.1. Source Positions and Uncertainties

The astrometric coordinates of the source positions were extracted from the mosaics by the centroiding routines built into *SExtractor 2.4.4*. The position of each source was taken from the mosaic that had the most significant detection. More than 300 of the sources in the 3rd IBIS/ISGRI catalog have well defined positions in the SIMBAD/NED database. Measuring the angular distance between the measured positions and those provided by the SIMBAD database gives an indication of the source position errors.

The point source location error of IBIS is highly dependent upon the significance of the source detected (Gros et al. 2003). By binning together sources of similar significance and calculating the mean source position error we can see how the source position accuracy varies with significance; this is shown in Figure 3, which also shows the empirical model derived by Gros et al. (2003):

$$\delta x = 22.1\sigma^{-0.95} + 0.16 \quad (1)$$

δx is the error in the source position (90% confidence, in arc minutes) and σ is the source significance. It is clear that the positions in this catalog are consistent with the expected scientific imaging performance of IBIS/ISGRI, and no additional systematic effects are introduced during our processing.

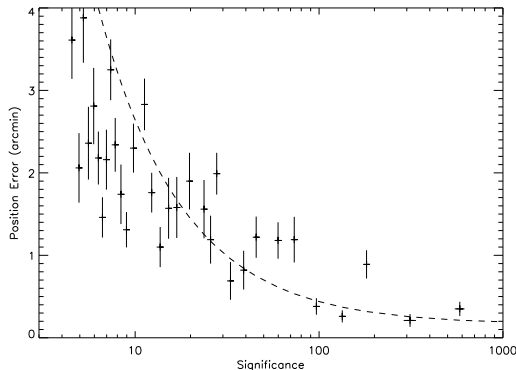


FIG. 3.— The binned mean source position error of sources as a function of source significance. Each bin contains 10 sources. The dashed line represents the model shown in Equation 1.

Compared to the second IBIS/ISGRI catalog, the position determination has been improved in several ways: the source positions are *always* taken from the mosaic in which they have the greatest significance; the use of multiple map projections has minimised the distortion of source PSFs; and the mosaics themselves are generated at higher resolution.

4.2. Fluxes and significances

The fluxes quoted in the table are the time-averaged fluxes over the whole dataset in two energy bands (20–40 and 40–100 keV). The significances quoted are the highest significance in any single map (also identified in the table), since this gives the best indication of the robustness of source detection. However, it should be noted therefore that the flux and significance values may derive from very different subsets of the data, and may initially appear contradictory.

5. DISCUSSION

We have derived an ‘unbiased’ catalog of 421 sources observed in a systematic analysis of the IBIS/ISGRI Core Programme and public data spanning nearly 3.5 years of operations.

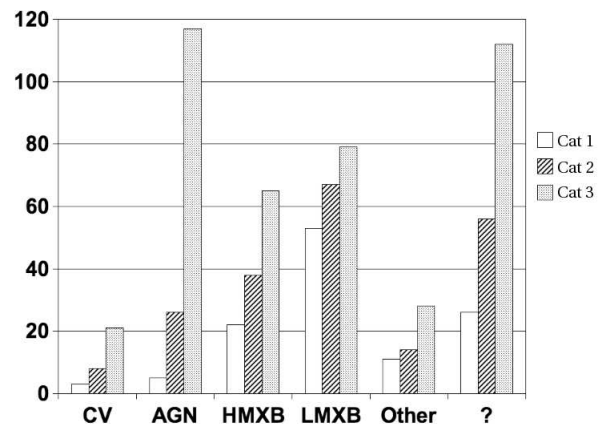


FIG. 4.— Numbers of sources in the 1st, 2nd and 3rd IBIS/ISGRI catalogs, classified by type.

Figure 4 illustrates a simple breakdown of the sources presented in this catalog by source type, and how this breakdown compares to previous catalogs. Note that we only include firm source type determinations in the following analysis, sources are not characterised based on their hard X-ray characteristics alone, but based on multi-waveband analysis. In the case of candidate AGN, an extragalactic nature is strongly indicated by multiwaveband analysis using radio, infra-red and X-ray archival data, by which their optical counterpart has been found to be associated with a galaxy.

This catalog is composed of 421 sources of which 171 are galactic accreting systems (corresponding to 41%), 122 are extragalactic objects (29%), 15 are of other types, and 113 (26%) are still not firmly classified.

Compared to the second catalog (Bird et al. 2006), the most dramatic change is the increase in AGN number, largely due to the increased exposure away from the Galactic Plane. This is also reflected in the increased CV detections, although in this case, it is because we are sampling a local approximately spherical distribution of objects within ~ 400 pc.

For galactic sources, this implies we have now detected more than half of the sources reported in the 2–10 keV band in the catalogs of Liu et al. (2000) and Liu et al. (2001). Taking the HMXB as an example, the number of

known HMXB was 30 in 1983 (van Paradijs et al. 1983), increasing to 69 in 1995 (van Paradijs et al. 1995), and increasing further to 130 in 2001 (Liu et al. 2001). Most of the new sources were identified with Be/X ray binaries and some were only tentatively identified as High or Low Mass on the basis of transient characteristic or spectral behaviour. This catalog, extending up to 100 keV, includes 68 firm HMXBs, implying not only detection of known sources but also that a large number (19 in total) of the new INTEGRAL sources are being identified with such systems. This is somewhat different to the results of 6 years of BeppoSAX/WFC operations, which detected predominantly outbursts from LMXB systems. While INTEGRAL continues to detect LMXBs, the rate of discovery is much lower than for the high-mass systems.

The percentage of sources without a firm identification has remained almost constant since the first IBIS/ISGRI catalog, at $\sim 25\%$. This is despite an active and successful campaign of follow-up observations in other wavebands (Masetti et al. (2006) and references therein). Of the 110 unclassified sources, around 25% have unconfirmed or ‘tentative’ classifications. INTEGRAL Gamma-ray (IGR) sources, represent detections that are either entirely new or those with no obvious counterpart or association in the hard X-ray and/or gamma-ray wavebands. There is a total of 167 IGRs in the third catalog, of which 69 have been firmly classified, predominantly as AGN, HMXB and intermediate polar CVs. The percentage of IGRs which have now been classified rises to $\sim 55\%$ if the tentative classifications are included.

Finally, we point out some interesting features of this catalog. Firstly, we have detected 21 CVs of which 9 are new detections and remarkably, for most of them emission is extended up to 100 keV. Secondly, we see the emergence of the supergiant fast X-ray transient (SFXT) class. The search for identification of IGRs sources has resulted in 8 firm associations and 4 possible ones. Also, there are at least 3 sources that have been observed not in coincidence with any recurrence time and reported either by Swift/XRT or Chandra. This implies the sources are rather persistent HMXB with luminous flares such as the HMXB supergiant neutron star systems 4U 1907+097 (Atel 915).

Finally, we note that 5 of the sources listed in the second IBIS/ISGRI catalog are not detected in this analysis, although this may be due to source variability in at least some cases.

5.1. Concluding comments

The positions derived from IBIS are forming the basis for an active program of follow-up observations in other wavebands, mainly X-ray (XMM-Newton, Chandra, RXTE and Swift), optical, IR and radio. The IBIS survey team, including scientists from five different institutes, will continue to refine the analysis techniques and apply them to the ever-increasing IBIS dataset. Further catalogs are expected to be released whenever the dataset and/or analysis tools justify them.

This is a golden age for high energy astronomy. The survey capabilities of IBIS/ISGRI and Swift/BAT are providing exceptional coverage of the soft gamma-ray sky, and intriguing links are now being found with the TeV sky being explored by CANGAROO, HESS, MAGIC and VERITAS. These telescopes will soon be joined by AGILE and GLAST, providing coverage over 15 orders of magnitude in energy from keV to TeV. Furthermore, the sources now being discovered will form the vital input catalogs for the next generations of narrow-field instruments such as Simbol-X in the X-ray domain and GRI at gamma-ray energies.

We acknowledge the following funding: in Italian Space Agency financial and programmatic support via contracts I/R/046/04 and ASI/INAF I/023/05/0; in UK via PPARC grant PP/C000714/1; in France, we thank CNES for support during ISGRI development and INTEGRAL data analysis. This research has made use of: data obtained from the High Energy Astrophysics Science Archive Research Center (HEASARC) provided by NASA’s Goddard Space Flight Center; the SIMBAD database operated at CDS, Strasbourg, France; the NASA/IPAC Extragalactic Database (NED) operated by the Jet Propulsion Laboratory, California Institute of Technology, under contract with the National Aeronautics and Space Administration.

REFERENCES

- Bélangier, G., Goldwurm, A., Renaud, M., et al. 2006, ApJ, 636, 275
 Bertin, E. & Arnouts, S. 1996, A&AS, 117, 393
 Bird, A.J., Barlow, E.J., Bassani, L., et al. 2004, ApJ, 607, 33
 Bird, A.J., Barlow, E.J., Bassani, L., et al., 2006, ApJ, 636, 765
 Goldwurm, A. et al. 2003, A&A, 411, L223
 Gros, A., Goldwurm, A., Cadolle-Bel, M., et al. 2003, A&A, 411, L179
 Lebrun, F., Leray, J.P., Lavocat, P., et al. 2003, A&A, 411, L141
 Liu, Q.Z., van Paradijs, J., van der Heuvel, E.P.J., et al. 2000, A&AS, 147, 25
 Liu, Q.Z., van Paradijs, J., van der Heuvel, E.P.J., et al. 2001, A&A, 368, 1021
 Masetti, N., Bassani, L., Bazzano, A. et al. 2006, A&A, 455, 11
 Ubertini, P., Lebrun, F., Di Cocco, G., et al. 2003, A&A, 411, L131
 van Paradijs, J. et al., 1983, A&A, 124, 294
 van Paradijs, J., in “X-ray binaries”, eds Lewin, W.H.G., van Paradijs, J. and van den Hevel, E.P.J., 1995, Cambridge, p536
 Winkler, C., et al. 2003, A&A, 411, L1

TABLE 1
3RD IBIS/ISGR1 CATALOG

Name ^a	RA	Dec	Error ^b	F20-40 ^c	F40-100 ^c	Type ^d	Signif ^e	Exposure ^f	MapCode ^g
IGR J00040+7020	1.006	70.336	3.8	0.8±0.1	0.9±0.3	AGN?	6.6	1237.0	B5
IGR J00234+6141	5.726	61.706	4.8	0.5±0.1	< 0.4	CV,IP	5.2	1841.0	S142B1
IGR J00245+6251	6.115	62.843	2.3	0.2±0.1	< 0.4	GRB	11.5	1823.0	R266B1
4U 0022+63	6.319	64.159	3.6	0.7±0.1	0.7±0.2	SNR	7.1	1756.0	B5
IGR J00256+6821	6.394	68.348	4.5	0.5±0.1	1.1±0.2	AGN?	5.5	1474.0	B3
V709 Cas	7.204	59.306	0.9	4.4±0.1	2.5±0.2	CV,IP	36.4	1765.0	B5
IGR J00291+5934	7.253	59.566	0.5	4.6±0.1	5.1±0.2	LMXB,msecXP,T	78.0	1752.0	R262B1
IGR J00333+6122	8.360	61.457	4.0	0.7±0.1	0.7±0.2	?	6.2	1777.0	B5
1ES 0033+59.5	8.985	59.829	2.8	1.1±0.1	1.1±0.2	AGN,BL Lac	9.4	1729.0	B4
IGR J00370+6122	9.264	61.371	4.1	0.5±0.1	< 0.4	HMXB,SG?	6.1	1731.0	R147B1
RX J0053.8-7226	13.543	-72.429	3.4	3.1±0.4	1.6±0.7	HMXB,XP,Be,T	7.7	132.0	B1
gam Cas	14.158	60.714	0.9	4.4±0.1	1.3±0.2	HMXB,Be	34.4	1503.0	B4
SMC X-1	19.283	-73.448	0.4	38.4±0.4	8.3±0.7	HMXB,XP	100.2	139.0	B4
1A 0114+650	19.500	65.289	0.6	9.9±0.1	4.8±0.3	HMXB,XP	64.4	1187.0	B5
4U 0115+634	19.619	63.743	0.2	42.5±0.1	11.8±0.3	HMXB,XP,T	792.2	1189.0	R238B2
IGR J01363+6610	24.019	66.166	3.7	< 0.4	< 0.6	HMXB,Be,T	6.9	916.0	R185B2
4U 0142+614	26.631	61.747	1.9	1.9±0.2	3.9±0.3	AXP	14.7	749.0	B3
RX J0146.9+6121	26.745	61.354	2.0	2.7±0.2	1.3±0.3	HMXB,XP,Be,T?	13.6	732.0	B5
IGR J01528-0326	28.254	-3.441	4.0	0.9±0.2	2.2±0.4	AGN,Sy2	6.3	575.0	B3
NGC 788	30.267	-6.822	1.8	2.9±0.2	3.0±0.4	AGN,Sy2	15.5	594.0	B5
IGR J02097+5222	32.408	52.412	5.1	1.9±0.4	1.5±0.7	AGN,Sy1	4.9	209.0	B5
SWIFT J0216.3+5128	34.137	51.431	5.0	1.3±0.5	2.9±0.7	AGN,Sy2	5.0	193.0	B3
NGC 985	38.677	-8.804	4.7	0.6±0.2	1.8±0.4	AGN,Sy1	5.3	435.0	B2
GT 0236+610	40.145	61.242	3.6	1.6±0.3	2.4±0.5	HMXB,microQSO	7.1	324.0	B5
NGC 1052	40.241	-8.242	4.4	1.3±0.2	< 0.9	AGN,Sy2	5.6	407.0	B5
RBS 345	40.567	5.530	5.5	0.8±0.3	1.5±0.5	AGN,Sy1	4.5	444.0	B5
NGC 1068	40.689	0.016	2.8	1.6±0.2	1.9±0.4	AGN,Sy2	9.2	589.0	B3
QSO B0241+62	41.285	62.480	2.3	3.4±0.3	4.0±0.6	AGN,Sy1	11.4	283.0	B3
IGR J02504+5443	42.604	54.721	4.1	1.6±0.3	2.1±0.5	AGN?	6.1	285.0	B5
MCG-02-08-014^h	43.120	-8.485	4.5	1.2±0.3	< 1.1	AGN,Sy2	5.5	330.0	B5
NGC 1142	43.771	-0.204	2.5	2.7±0.3	3.4±0.5	AGN,Sy2	10.6	402.0	B3
B3 B0309+411B	48.273	41.343	4.1	1.9±0.3	< 1.2	AGN,Sy1/RG	6.1	218.0	B5
IGR J03184-0014ⁱ	49.600	-0.229	4.0	3.8±0.7	< 2.2	AGN,QSO/BAL	6.3	81.0	B4
NGC 1275	49.953	41.517	2.6	3.1±0.4	1.5±0.6	AGN,Sy2	10.1	211.0	B4
1H 0323+342	51.088	34.178	4.3	2.5±0.5	2.4±0.9	AGN,Sy1	5.9	99.0	B5
GK Per	52.778	43.934	4.1	1.4±0.3	1.1±0.6	CV,IP	6.2	270.0	R273B2
EXO 0331+530	53.741	53.169	0.2	214.6±0.3	44.0±0.5	HMXB,XP,Be,T	920.5	333.0	R273B2
IGR J03532-6829	58.308	-68.483	3.6	< 0.9	< 1.5	AGN,RG	7.1	151.0	S012B3
X Per	58.835	31.049	1.0	26.4±1.0	31.8±1.7	HMXB,XP,Be	30.5	51.0	B5
3C 111	64.573	38.014	3.1	4.9±0.7	6.1±1.2	AGN,Sy1/BLRG	8.5	72.0	B5
LEDA 168563	73.028	49.514	3.0	3.6±0.5	3.8±0.8	AGN,Sy1	8.6	135.0	B5
ESO 33-2	73.918	-75.602	5.4	1.7±0.3	1.3±0.6	AGN,Sy2	4.5	230.0	B3
IGR J05053-7343	76.329	-73.716	3.6	1.0±0.3	< 1.2	?	7.0	229.0	R028B1
4U 0517+17	77.676	16.477	3.0	3.6±0.4	3.8±0.6	AGN,Sy1.5	8.8	233.0	B3
IGR J05270-6631	81.756	-66.511	4.4	1.3±0.3	< 1.2	?	5.7	207.0	B4
LMC X-4	83.212	-66.368	0.4	48.0±0.3	15.6±0.6	HMXB,XP	144.6	203.0	B1
Crab	83.629	22.018	0.2	1000	1000	PWN,PSR	4529.5	572.0	B5
1A 0535+262	84.732	26.358	2.8	3.0±0.3	2.0±0.4	HMXB,XP,Be,T	9.4	404.0	B1
LMC X-1	84.903	-69.749	1.1	< 0.6	< 1.1	HMXB,BH	26.3	219.0	S012B3
PSR B0540-69.3	85.057	-69.297	3.9	1.9±0.3	1.9±0.6	XB,XP	6.5	221.0	B3
BY Cam	85.737	60.850	4.8	2.7±0.5	2.2±0.9	CV,P	5.2	161.0	B4
MCG+08-11-011	88.717	46.442	3.8	4.4±0.8	3.1±1.4	AGN,Sy1.5	6.6	44.0	B5
SWIFT J0601.9-8636	91.838	-86.571	5.2	1.4±0.4	2.3±0.7	AGN,Sy2?	4.8	152.0	R099B2
PKS 0611-663	92.938	-66.433	4.6	1.1±0.3	2.2±0.6	AGN	5.5	191.0	B3
Mrk 3	93.891	71.043	1.2	4.9±0.2	6.8±0.4	AGN,Sy2	25.1	547.0	B5
4U 0614+091	94.280	9.139	0.8	26.8±0.7	22.1±1.1	LMXB,B,A	39.2	83.0	B5
IGR J06239-6052^j	95.978	-60.898	4.9	2.5±0.5	2.1±0.8	?	5.1	112.0	B5
IGR J06253+7334	96.340	73.602	5.2	0.8±0.2	< 0.9	CV,IP	4.7	545.0	B4
IGR J06292+4858	97.301	48.974	5.0	8.8±1.8	< 6.0	?	4.9	14.0	B1
Mrk 6	103.032	74.423	2.0	2.4±0.2	3.4±0.4	AGN,Sy1.5	14.0	578.0	B5
IGR J07295-1329	112.376	-13.158	5.4	1.9±0.5	< 1.8	?	4.5	116.0	B5
IGR J07437-5137	115.920	-51.617	5.0	1.2±0.2	< 0.7	?	5.0	548.0	B5
EXO 0748-676	117.149	-67.754	0.8	21.7±0.6	18.1±1.0	LMXB,B,D,T	43.7	116.0	B5
IGR J07565-4139	119.110	-41.631	3.8	1.2±0.2	0.9±0.3	AGN,Sy2	6.8	968.0	B4
IGR J07597-3842	119.923	-38.719	2.3	2.2±0.2	2.3±0.3	AGN,Sy1.2	11.8	837.0	B5
ESO 209-12	120.507	-49.753	3.6	0.9±0.2	1.7±0.3	AGN,Sy1.5	7.2	936.0	B5
QSO B0804+761	122.781	76.010	5.2	0.9±0.2	< 0.9	AGN,Sy1	4.7	528.0	B5
Vela Pulsar	128.831	-45.182	0.6	7.1±0.1	8.1±0.2	PWN,PSR	65.5	1556.0	B5
4U 0836-429	129.346	-42.894	0.2	31.2±0.1	26.6±0.2	LMXB,B,T	378.5	1576.0	S137B3
FRL 1146	129.620	-36.013	3.5	1.2±0.2	0.9±0.3	AGN,Sy1.5	7.4	1041.0	B5
IGR J08408-4503	130.203	-45.061	5.3	< 0.2	0.5±0.2	HMXB,SFXT	4.6	1643.0	B3
QSO B0836+710	130.296	70.897	2.0	2.6±0.2	3.8±0.4	AGN,Blazar	13.4	506.0	B5
Vela X-1	135.523	-40.554	0.2	221.0±0.1	51.1±0.2	HMXB,XP	1554.0	1527.0	B1
IGR J09025-6814	135.612	-68.235	5.1	1.2±0.3	1.7±0.5	?	4.8	381.0	S192B3
IGR J09026-4812	135.668	-48.216	2.3	1.3±0.1	1.4±0.2	?	11.5	1527.0	B5

TABLE 1
3RD IBIS/ISGRI CATALOG

IGR J09103-3741	137.577	-37.675	5.2	< 0.3	< 0.5	?	4.7	965.0	S315B1
SWIFT J0917.2-6221	139.040	-62.314	3.0	1.5±0.2	1.1±0.3	AGN,Sy1	8.7	998.0	B5
EXMS B0918-549E	140.051	-55.125	4.1	3.0±0.2	2.2±0.3	?,T	6.2	1317.0	R139B1
4U 0919-54	140.093	-55.191	1.1	4.0±0.2	3.0±0.3	LMXB	26.4	1306.0	B5
IGR J09253+6929	141.320	69.488	4.7	1.4±0.3	< 1.2	?	5.3	290.0	B5
IGR J09469-4603	146.722	-46.046	4.8	0.7±0.2	0.9±0.3	?	5.1	1199.0	B3
MCG-05-23-016	146.916	-30.936	1.9	9.2±0.6	8.0±1.0	AGN,Sy2	15.0	90.0	B5
IGR J09485-4726	147.120	-47.427	4.9	0.5±0.2	1.3±0.3	?	5.1	1158.0	B3
IGR J09523-6231	148.069	-62.516	3.9	0.9±0.1	0.6±0.3	?	6.4	1227.0	B5
SWIFT J1009.3-4250	152.393	-42.784	3.3	1.8±0.3	1.6±0.4	AGN,Sy2	7.8	600.0	B5
GRO J1008-57	152.434	-58.296	0.5	4.6±0.1	2.1±0.2	HMXB,XP,Be,T	74.5	1571.0	R203B1
IGR J10101-5654	152.523	-56.916	2.8	1.1±0.1	0.6±0.2	HMXB	9.3	1520.0	B5
IGR J10109-5746	152.666	-57.788	2.7	1.1±0.1	< 0.4	Symb	9.7	1585.0	B4
IGR J10147-6354	153.677	-63.892	5.0	< 0.3	1.3±0.2	?	4.9	1340.0	B3
NGC 3281	157.951	-34.869	3.9	2.3±0.5	3.6±0.9	AGN,Sy2	6.5	110.0	B5
4U 1036-56	159.373	-56.784	3.5	0.8±0.1	< 0.4	HMXB,Be	7.3	1555.0	S081B3
SWIFT J1038.8-4942	159.652	-49.829	4.0	0.8±0.2	0.9±0.3	AGN,Sy1.5	6.3	1016.0	B5
IGR J10404-4625	160.107	-46.410	3.1	1.9±0.2	1.9±0.4	AGN,Sy2	8.3	626.0	B3
IGR J10448-5945^k	161.197	-59.755	5.2	0.3±0.1	0.9±0.2	?	4.8	1578.0	B3
IGR J11098-6457	167.442	-64.946	5.5	0.6±0.2	0.9±0.2	?	4.5	1252.0	B5
IGR J11187-5438	169.677	-54.633	4.0	1.0±0.1	0.8±0.2	?	6.3	1269.0	B1
Cen X-3	170.307	-60.627	0.2	64.3±0.1	7.2±0.2	HMXB,XP	542.9	1445.0	B4
IGR J11215-5952	170.450	-59.869	1.5	0.5±0.1	< 0.5	HMXB,SFXT	19.1	1422.0	S308B1
IGR J11305-6256	172.775	-62.939	1.2	3.9±0.1	1.7±0.2	HMXB,Be	26.1	1337.0	B5
IGR J11366-6002	174.158	-60.034	4.9	0.6±0.1	0.9±0.2	AGN?	5.0	1302.0	B3
NGC 3783	174.733	-37.745	3.2	10.5±1.2	5.8±2.2	AGN,Sy1	8.1	23.0	B1
EXMS B1136-650	174.870	-65.405	3.2	< 0.3	< 0.5	RSCVn	8.0	1203.0	R088B1
IGR J11435-6109	175.969	-61.145	2.6	1.2±0.2	0.9±0.2	HMXB,XP?,Be	10.4	1292.0	R258B2
1E 1145.1-6141	176.864	-61.963	0.3	26.7±0.2	15.7±0.3	HMXB,XP	172.2	1305.0	B5
2E 1145.5-6155	176.981	-62.187	1.0	4.0±0.2	2.4±0.3	HMXB,XP	31.6	1282.0	R076B2
IGR J12026-5349	180.642	-53.849	2.2	2.5±0.2	2.2±0.3	AGN,Sy2	12.3	728.0	B3
NGC 4138	182.393	43.676	5.3	2.5±0.6	2.9±1.1	AGN,Sy1.9	4.6	62.0	B5
NGC 4151	182.636	39.409	0.4	33.7±0.6	40.2±1.0	AGN,Sy1.5	144.0	71.0	STB1
EXMS B1210-645	183.272	-64.897	4.9	0.7±0.2	0.6±0.2	?,T	5.0	1168.0	B5
NGC 4180^l	183.291	7.009	5.2	0.6±0.2	1.6±0.4	AGN	4.7	622.0	B3
4C 04.42	185.612	4.256	3.2	1.0±0.2	2.0±0.3	AGN,QSO	8.0	810.0	B3
Mrk 50	185.862	2.693	3.4	1.1±0.2	0.6±0.3	AGN,Sy1	7.6	848.0	B4
NGC 4395	186.364	33.556	5.4	1.5±0.4	1.8±0.7	AGN,Sy1.8	4.6	144.0	B5
NGC 4388	186.445	12.658	0.7	12.4±0.3	15.2±0.5	AGN,Sy2	53.1	411.0	B5
GX 301-2	186.649	-62.772	0.2	134.0±0.2	17.9±0.3	HMXB,XP,T	786.1	1038.0	B4
XSS J12270-4859	187.007	-48.893	4.3	1.8±0.3	1.7±0.5	CV,IP	5.9	336.0	B5
3C 273	187.280	2.049	0.6	10.1±0.2	11.5±0.3	AGN,QSO	69.0	892.0	B5
IGR J12349-6434	188.722	-64.570	1.2	4.4±0.2	3.3±0.3	Symb	24.6	965.0	B5
NGC 4507	188.908	-39.904	1.1	8.9±0.4	11.3±0.7	AGN,Sy2	27.6	215.0	B5
ESO 506-G27	189.748	-27.237	5.1	4.8±1.1	< 0.3	AGN,Sy2	4.9	28.0	B5
LEDA 170194	189.778	-16.190	3.3	2.4±0.4	4.6±0.7	AGN,Sy2	7.8	200.0	B3
NGC 4593	189.905	-5.353	1.1	4.2±0.2	4.3±0.3	AGN,Sy1	27.0	817.0	B5
IGR J12415-5750	190.377	-57.825	3.7	1.4±0.2	1.3±0.3	AGN,Sy2	6.8	727.0	B5
1H 1249-637	190.725	-63.049	4.0	1.1±0.2	< 0.6	HMXB,Be	6.3	963.0	B4
4U 1246-58	192.410	-59.090	1.6	3.1±0.2	2.4±0.3	LMXB,B	17.2	848.0	B5
ESO 323-32	193.394	-41.626	4.7	0.9±0.3	1.6±0.5	AGN,Sy2	5.3	322.0	B5
3C 279	194.037	-5.742	3.5	0.9±0.2	1.8±0.3	AGN,Blazar	7.3	685.0	B3
1H 1254-690	194.438	-69.288	1.6	2.5±0.2	< 0.7	LMXB,B,D	17.2	711.0	B4
Coma Cluster	194.884	27.939	2.9	1.8±0.3	< 1.0	Cluster	9.1	286.0	B4
IGR J13020-6359	195.537	-63.947	2.3	2.1±0.2	1.4±0.3	HMXB,XP,Be	11.5	926.0	B5
NGC 4945	196.361	-49.470	0.6	13.7±0.2	20.7±0.4	AGN,Sy2	69.4	511.0	B3
ESO 323-77	196.621	-40.449	4.2	1.2±0.3	2.1±0.5	AGN,Sy1.2	6.0	346.0	B3
IGR J13091+1137	197.290	11.635	3.7	2.4±0.4	2.9±0.6	AGN,Sy2,XBONG	6.8	268.0	B3
IGR J13109-5552	197.682	-55.863	3.4	1.2±0.2	1.6±0.3	AGN?	7.4	762.0	B3
NGC 5033	198.348	36.571	4.9	1.3±0.3	< 1.2	AGN,Sy1.9	5.1	189.0	B5
IGR J13186-6257	199.652	-62.946	3.8	0.8±0.2	< 0.6	?	6.6	958.0	B5
Cen A	201.365	-43.020	0.3	38.1±0.2	48.4±0.4	AGN,Sy2	183.3	421.0	B5
4U 1323-62	201.634	-62.136	0.9	5.9±0.2	3.5±0.3	LMXB,B,D	35.7	992.0	B5
1RXS J133447.5+371100	203.793	37.199	4.2	2.1±0.4	< 1.5	XB	6.0	139.0	B4
MCG-06-30-015	203.995	-34.302	2.1	3.7±0.3	2.0±0.5	AGN,Sy1.2	13.1	325.0	B1
NGC 5252	204.559	4.504	4.6	3.5±0.6	< 2.1	AGN,Sy1.9	5.5	120.0	B1
4U 1344-60	206.883	-60.610	1.0	4.3±0.2	4.4±0.3	AGN,Sy1.5	29.5	1042.0	B5
IC 4329A	207.339	-30.309	0.8	12.0±0.3	13.2±0.6	AGN,Sy1.2	41.7	239.0	B5
IGR J14003-6326	210.154	-63.447	3.9	1.1±0.2	1.0±0.3	?	6.5	1052.0	B1
V834 Cen	212.249	-45.273	4.4	1.1±0.2	< 0.7	CV,P	5.7	726.0	B4
Circinus Galaxy	213.282	-65.345	0.5	14.1±0.2	11.7±0.3	AGN,Sy2	88.4	991.0	B5
NGC 5506	213.318	-3.197	2.1	6.3±0.5	4.3±0.9	AGN,Sy1.9	12.9	71.0	STB1
IGR J14175-4641	214.275	-46.676	5.5	0.5±0.2	1.1±0.4	AGN,Sy2	4.5	790.0	B3
ESO 511-G030	214.860	-26.644	4.0	2.2±0.4	1.9±0.8	AGN,Sy1	6.3	180.0	B5
IGR J14298-6715	217.338	-67.260	4.3	0.7±0.2	0.8±0.3	?	5.9	856.0	B5
IGR J14319-3315	217.988	-33.245	4.8	1.2±0.3	< 0.9	?	5.1	449.0	B1
IGR J14331-6112	218.357	-61.204	3.7	0.8±0.2	0.7±0.3	?	6.8	1216.0	B5

TABLE 1
3RD IBIS/ISGRI CATALOG

IGR J14471-6414^m	221.588	-64.294	4.6	0.6±0.2	0.8±0.3	?	5.4	1066.0	B5
IGR J14471-6319	221.872	-63.309	4.6	0.7±0.2	1.0±0.3	AGN,Sy2	5.5	1115.0	B5
IGR J14492-5535	222.358	-55.561	3.3	1.2±0.1	0.7±0.3	AGN	7.8	1427.0	B1
IGR J14515-5542	222.904	-55.669	3.4	0.9±0.1	1.0±0.3	AGN,Sy2	7.6	1453.0	B5
IGR J14532-6356	223.312	-63.927	5.3	< 0.3	< 0.6	?	4.6	1099.0	R036B1
IGR J14536-5522	223.435	-55.374	2.7	1.5±0.1	< 0.5	CV	9.9	1475.0	B1
IGR J14552-5133	223.792	-51.588	4.4	0.8±0.2	0.6±0.3	AGN,NL Sy1	5.6	1375.0	B5
IC 4518A	224.391	-43.156	2.3	1.6±0.2	1.1±0.3	AGN,Sy2	11.5	898.0	B5
IGR J15094-6649	227.351	-66.844	2.9	1.7±0.2	< 0.7	CV,IP	8.9	833.0	B1
PSR B1509-58	228.486	-59.147	0.5	9.0±0.1	10.9±0.2	PSR	70.6	1439.0	B5
ESO 328-IG036	228.755	-40.380	4.8	0.8±0.2	0.6±0.3	AGN,Sy1	5.2	931.0	B5
IGR J15161-3827	229.037	-38.448	5.3	0.5±0.2	1.2±0.3	AGN?	4.7	816.0	B2
Cir X-1	230.172	-57.169	0.4	9.3±0.1	0.6±0.2	LMXB,B,A,T	99.1	1557.0	B4
IGR J15359-5750	234.031	-57.803	2.5	1.1±0.1	1.5±0.2	?	10.5	1663.0	B5
4U 1538-522	235.595	-52.388	0.3	22.3±0.1	3.4±0.2	HMXB,XP	162.8	1999.0	B1
XTE J1543-568	236.010	-56.712	4.2	0.5±0.1	< 0.5	HMXB,XP,Be,T	6.0	1771.0	S047B1
4U 1543-624	236.976	-62.570	1.3	3.4±0.2	0.6±0.3	LMXB,NS?	23.0	1126.0	B4
IGR J15479-4529	237.050	-45.478	0.9	5.1±0.1	3.1±0.2	CV,IP	35.8	1622.0	B5
NGC 5995	237.113	-13.762	3.8	2.2±0.6	2.1±0.5	AGN,Sy2	6.7	138.0	B2
XTE J1550-564	237.745	-56.479	0.2	34.0±0.1	55.3±0.2	LMXB,BH,T	737.9	1821.0	S047B3
IGR J15529-5029	238.235	-50.490	3.9	0.9±0.1	< 0.4	?	6.5	2020.0	B5
IGR J15539-6142	238.336	-61.671	3.9	0.7±0.2	1.7±0.3	AGN?	6.4	1220.0	B3
1H 1556-605	240.312	-60.754	2.9	0.8±0.2	0.6±0.3	LMXB	9.1	1305.0	B4
IGR J16024-6107	240.609	-61.124	4.7	0.9±0.2	< 0.5	AGN?	5.2	1254.0	B1
IGR J16056-6110	241.394	-61.171	5.0	0.5±0.2	1.3±0.3	AGN	4.9	1229.0	B3
IGR J16119-6036	242.988	-60.658	2.6	1.5±0.2	1.5±0.3	AGN,Sy1	10.2	1263.0	B5
4U 1608-522	243.177	-52.424	0.4	13.9±0.1	7.8±0.2	LMXB,B,A,T	119.8	1984.0	B4
IGR J16167-4957	244.140	-49.974	1.7	2.1±0.1	0.7±0.2	CV,IP	16.3	2002.0	B4
PSR J1617-5055	244.303	-50.942	3.5	0.9±0.1	0.9±0.2	PSR	7.4	2007.0	B5
IGR J16185-5928	244.607	-59.446	3.8	1.2±0.2	1.0±0.3	AGN,NL Sy1	6.8	1314.0	B5
AX J1619.4-4945	244.895	-49.744	1.8	2.0±0.1	1.2±0.2	HMXB?,SFXT?	15.6	1964.0	B5
IGR J16194-2810	244.899	-28.138	3.5	2.5±0.3	1.2±0.4	?	7.4	461.0	B1
Sco X-1	244.980	-15.643	0.2	685.7±0.3	24.7±0.3	LMXB,Z	2422.7	423.0	B4
IGR J16207-5129	245.189	-51.505	1.2	3.3±0.1	2.3±0.2	HMXB,SG	26.0	1943.0	B5
IGR J16248-4603	246.207	-46.043	4.7	< 0.3	< 0.4	?	5.3	1864.0	S163B2
SWIFT J1626.6-5156	246.648	-51.944	2.0	< 0.3	0.4±0.2	LMXB?,XP,T	14.0	1884.0	R399B2
4U 1624-490	247.013	-49.208	0.7	4.4±0.1	0.4±0.2	LMXB,D	48.9	1933.0	B4
IGR J16283-4838	247.041	-48.644	3.3	0.7±0.1	0.5±0.2	HMXB?,NS?	7.8	1896.0	R303B2
IGR J16287-5021	247.174	-50.344	4.4	0.8±0.1	< 0.4	?	5.7	1916.0	B1
IGR J16318-4848	247.952	-48.820	0.3	24.8±0.1	12.8±0.2	HMXB	179.8	1945.0	B5
AX J1631.9-4752	248.006	-47.875	0.4	17.4±0.1	6.4±0.2	HMXB,XP,T	121.7	1830.0	B1
4U 1626-67	248.082	-67.468	0.6	18.4±0.3	1.8±0.5	LMXB,XP	65.3	445.0	B4
IGR J16328-4726	248.190	-47.437	4.5	4.0±0.1	3.2±0.2	?	5.6	1718.0	S351B3
4U 1630-47	248.507	-47.396	0.2	38.9±0.1	32.3±0.2	LMXB,BHC,D,T	407.5	1842.0	S100B1
IGR J16351-5806	248.796	-58.090	3.1	1.0±0.2	1.3±0.3	AGN,Sy2	8.3	1397.0	B5
IGR J16358-4726	248.976	-47.425	0.8	2.1±0.1	1.1±0.2	?,XP,T	40.3	1697.0	R052B1
IGR J16377-6423	249.557	-64.356	3.7	1.3±0.2	< 0.8	Cluster?	6.9	649.0	B4
IGR J16385-2057	249.626	-20.944	4.1	1.4±0.2	0.6±0.3	AGN	6.2	726.0	B3
AX J1639.0-4642	249.775	-46.706	0.7	6.3±0.1	0.7±0.2	HMXB,XP,T	48.7	1890.0	B4
4U 1636-536	250.228	-53.753	0.3	38.1±0.1	23.4±0.2	LMXB,B,A	272.1	1713.0	B5
IGR J16418-4532	250.468	-45.548	1.0	4.7±0.1	1.1±0.2	HMXB,XP,SFXT?	30.7	1847.0	B1
IGR J16426+6536	250.656	65.594	4.5	3.1±0.6	< 2.1	?	5.5	97.0	R206B1
GX 340+0	251.448	-45.614	0.2	31.9±0.1	1.5±0.2	LMXB,Z	332.6	1920.0	B4
IGR J16460+0849	251.489	8.818	5.2	6.8±2.4	12.6±3.8	?	4.7	11.0	B3
IGR J16465-4507	251.696	-45.125	2.1	1.8±0.1	1.1±0.2	HMXB,SFXT?,XP	12.8	1916.0	R222B2
IGR J16479-4514	252.015	-45.216	1.4	4.5±0.1	2.4±0.2	HMXB,SFXT?	20.2	1950.0	B2
IGR J16482-3036	252.062	-30.590	2.2	1.7±0.2	1.9±0.2	AGN,Sy1	12.4	1723.0	B3
IGR J16493-4348	252.375	-43.828	1.7	2.3±0.1	1.6±0.2	LMXB?	16.8	2053.0	B5
IGR J16500-3307	252.491	-33.064	2.4	1.8±0.2	0.5±0.2	?	11.3	1943.0	B1
ESO 138-1ⁿ	253.049	-59.222	3.8	1.3±0.2	1.1±0.3	AGN,Sy2	6.8	1066.0	B5
NGC 6221^o	253.049	-59.222	3.8	1.3±0.2	1.1±0.3	AGN,Sy1/Sy2	6.8	1066.0	B5
GRO J1655-40	253.504	-39.846	0.6	2.3±0.1	2.7±0.2	LMXB,BH,T	58.9	2406.0	S296B3
IGR J16558-5203	254.010	-52.062	2.0	1.8±0.1	2.1±0.2	AGN,Sy1.2	13.9	1509.0	B3
Swift J1656.3-3302	254.110	-33.047	2.5	1.2±0.1	1.5±0.2	AGN?	10.6	2314.0	B3
Her X-1	254.461	35.339	2.7	87.0±9.0	< 20.0	LMXB,XP	9.6	2.0	STB1
AX J1700.2-4220	255.059	-42.308	2.0	1.9±0.1	1.5±0.2	HMXB	14.1	1991.0	B5
OXO 1657-415	255.203	-41.659	0.2	76.7±0.1	40.4±0.2	HMXB,XP	529.1	2223.0	B5
IGR J17008-6425	255.204	-64.425	4.5	1.2±0.3	1.6±0.5	?	5.6	499.0	B5
XTE J1701-462	255.232	-46.182	1.1	0.6±0.1	< 0.4	LMXB,Z,T	26.3	1761.0	R411B2
GX 339-4	255.706	-48.792	0.3	40.7±0.1	46.7±0.2	LMXB,BH,T	306.3	1590.0	B3
4U 1700-377	255.987	-37.847	0.2	208.1±0.1	123.8±0.2	HMXB	1670.4	3106.0	B5
GX 349+2	256.441	-36.426	0.2	48.7±0.1	1.1±0.2	LMXB,Z	574.5	3120.0	B4
4U 1702-429	256.559	-43.041	0.4	15.2±0.1	9.1±0.2	LMXB,B,A	108.5	2089.0	B5
1H 1705-250	257.065	-25.094	5.0	0.5±0.1	< 0.3	LMXB,BHC,T	5.0	2555.0	S411B3
IGR J17088-4008	257.220	-40.164	2.3	1.2±0.1	2.4±0.2	AXP	11.8	2665.0	B3
4U 1705-32	257.221	-32.315	1.2	2.8±0.1	2.7±0.2	LMXB,B	24.4	3340.0	B3
4U 1705-440	257.223	-44.105	0.3	28.3±0.1	13.1±0.2	LMXB,B,A	207.1	1940.0	B4

TABLE 1
3RD IBIS/ISGRI CATALOG

IGR J17091-3624	257.280	-36.407	0.5	6.7±0.1	8.9±0.2	XB,BHC?	74.6	3134.0	S163B3
XTE J1709-267	257.393	-26.651	1.8	0.8±0.1	0.7±0.2	LMXB,B,T	15.9	2758.0	R171B1
IGR J17098-3628	257.462	-36.463	1.9	2.9±0.1	2.9±0.2	?,BHC?,T	14.4	3028.0	S301B3
XTE J1710-281	257.539	-28.123	1.1	3.0±0.1	3.0±0.2	LMXB,B,T	29.1	3040.0	B3
4U 1708-40	258.104	-40.859	2.3	1.1±0.1	0.6±0.2	LMXB,B	12.0	2534.0	B4
Oph Cluster	258.112	-23.348	0.8	5.2±0.1	1.1±0.2	Cluster	41.9	2869.0	B4
SAX J1712.6-3739	258.137	-37.645	0.8	4.7±0.1	4.0±0.2	LMXB,B,T	41.0	3263.0	B5
V2400 Oph	258.172	-24.280	1.2	3.5±0.1	1.0±0.2	CV,IP	24.3	2765.0	B1
XTE J1716-389	258.915	-38.875	3.5	1.0±0.1	0.6±0.2	HMXB,SG	7.4	3003.0	B4
NGC 6300	259.229	-62.822	1.8	4.4±0.3	3.6±0.5	AGN,Sy2	15.2	494.0	B5
IGR J17195-4100	259.906	-41.014	1.7	2.4±0.1	1.5±0.2	CV,IP	16.9	2531.0	B5
XTE J1720-318	259.995	-31.760	0.7	1.7±0.1	2.7±0.1	LMXB,BHC,T	53.8	4127.0	S047B3
IGR J17200-3116	260.025	-31.284	1.1	2.8±0.1	1.2±0.1	HMXB,T	26.5	4192.0	B5
IGR J17204-3554	260.104	-35.892	2.0	1.1±0.1	2.0±0.2	AGN?	14.0	3620.0	B3
EXO 1722-363	261.299	-36.282	0.5	10.3±0.1	3.0±0.2	HMXB,XP	91.8	3744.0	B1
IGR J17254-3257	261.361	-32.971	1.3	2.2±0.1	2.1±0.1	LMXB,B	23.2	4513.0	B5
IGR J17269-4737	261.755	-47.622	3.7	< 0.3	0.5±0.3	?,T	6.8	1285.0	S358B1
GRS 1724-308	261.891	-30.805	0.3	19.4±0.1	15.7±0.1	LMXB,G,B,A	223.8	4626.0	B5
IGR J17285-2922	262.143	-29.375	3.5	< 0.2	< 0.3	XB?,T	7.2	4381.0	R120B1
IGR J17303-0601	262.596	-5.988	1.9	3.8±0.3	2.7±0.4	CV,IP	14.7	498.0	B5
IGR J17314-2854	262.853	-28.895	3.2	0.3±0.1	0.5±0.1	?	8.0	4775.0	S100B3
GX 9+9	262.933	-16.963	0.4	14.1±0.1	0.5±0.2	LMXB,A	141.5	2098.0	B4
V2487 Oph	262.963	-19.233	3.1	0.8±0.1	0.8±0.2	CV,IP?	8.5	2635.0	B5
GX 354-0	262.991	-33.834	0.2	41.1±0.1	14.1±0.1	LMXB,B,A	471.6	4550.0	B4
GX 1+4	263.008	-24.747	0.2	50.6±0.1	39.1±0.1	LMXB,XP	544.3	4161.0	B5
IGR J17331-2406	263.306	-24.156	1.8	0.6±0.1	0.8±0.1	?	15.4	4191.0	S227B3
4U 1730-335	263.351	-33.386	0.5	5.9±0.1	2.6±0.1	LMXB,G,RB,T	81.1	4549.0	S100B1
IGR J17348-2045	263.699	-20.750	4.3	< 0.2	0.7±0.2	?	5.8	3348.0	R230B2
IGR J17354-3255	263.839	-32.937	2.2	1.2±0.1	0.7±0.1	?	12.5	4436.0	B5
GRS 1734-292	264.377	-29.137	0.6	5.5±0.1	4.5±0.1	AGN,Sy1	67.0	4858.0	B5
IGR J17379-3747	264.473	-37.783	5.3	0.3±0.1	0.4±0.2	?	4.6	3134.0	R164B1
SLX 1735-269	264.572	-26.993	0.4	10.3±0.1	8.6±0.1	LMXB,B	123.5	4662.0	B5
4U 1735-444	264.741	-44.452	0.3	29.9±0.2	0.9±0.2	LMXB,B,A	231.6	1411.0	B4
XTE J17391-3021	264.800	-30.349	1.2	1.5±0.1	0.8±0.1	HMXB,SFXT,Be?	24.0	5132.0	R106B1
AX J1739.3-2923	264.875	-29.370	4.9	0.3±0.1	0.5±0.1	?	5.1	4858.0	B2
XTE J1739-285	264.985	-28.488	1.1	1.5±0.1	0.9±0.1	LMXB,B,T	26.3	4870.0	R362B2
IGR J17404-3655	265.112	-36.913	3.5	0.8±0.1	0.7±0.2	?	7.3	3139.0	B5
IGR J17407-2808	265.173	-28.202	4.2	2.2±0.1	2.6±0.1	?,SFXT?	6.0	4639.0	R243B1
SLX 1737-282	265.179	-28.291	1.3	3.7±0.1	3.8±0.1	LMXB,B	22.5	4699.0	S227B3
2E 1739.1-1210	265.474	-12.215	2.7	1.4±0.2	1.8±0.3	AGN,Sy1	9.9	1274.0	B5
IGR J17419-2802	265.486	-28.034	2.0	0.3±0.1	0.3±0.1	?,T	13.4	4482.0	R362B1
IGR J17426-0258	265.645	-2.963	4.3	< 0.5	< 0.9	?	5.9	526.0	R429B1
XTE J1743-363	265.747	-36.377	1.1	3.2±0.1	2.5±0.1	?	27.0	3213.0	B5
1E 1740.7-2942	265.978	-29.750	0.2	29.8±0.1	36.6±0.1	LMXB,BHC	486.3	5143.0	S100B3
IGR J17445-2747	266.120	-27.756	2.3	0.5±0.1	0.4±0.1	?	11.9	4383.0	S163B3
IGR J17448-3232	266.229	-32.550	2.2	0.8±0.1	0.5±0.1	?	12.4	4920.0	B4
KS 1741-293	266.234	-29.352	0.6	5.2±0.1	4.2±0.1	LMXB,B,T	67.2	5174.0	B5
IGR J17456-2901 ^P	266.410	-29.021	0.6	5.3±0.1	2.9±0.1	?	65.2	5203.0	B5
1A 1742-294	266.523	-29.517	0.8	14.8±0.1	7.5±0.1	LMXB,B	39.2	5188.0	R411B1
IGR J17461-2853^d	266.523	-28.882	0.6	5.5±0.1	3.1±0.1	mol cloud?	65.5	5096.0	B5
IGR J17461-2204	266.533	-22.059	3.7	0.5±0.1	0.5±0.1	?	6.8	4165.0	B4
IGR J17464-3213	266.565	-32.233	0.2	27.8±0.1	20.9±0.1	LMXB,BHC,T	658.9	4858.0	S047B1
1E 1743.1-2843 ^f	266.580	-28.735	0.6	5.5±0.1	2.1±0.1	LMXB?	65.7	4913.0	B4
SAX J1747.0-2853	266.712	-28.888	0.9	3.6±0.1	1.9±0.1	LMXB,B,T	38.0	5019.0	S411B1
IGR J17472+0701	266.797	7.018	5.3	2.3±0.4	< 1.5	?	4.6	192.0	B1
IGR J17473-2721	266.819	-27.348	4.7	< 0.2	0.5±0.1	?,T	5.3	4691.0	S308B1
IGR J17475-2822	266.830	-28.400	1.0	2.5±0.1	2.1±0.1	mol cloud?	33.0	4964.0	B5
SLX 1744-299	266.858	-30.021	0.4	9.5±0.1	5.7±0.1	LMXB,B	114.3	5164.0	B5
IGR J17476-2253	266.906	-22.887	1.8	1.3±0.1	1.5±0.1	AGN?,QSO?	15.3	4424.0	B3
GX 3+1	266.980	-26.562	0.3	11.7±0.1	0.9±0.1	LMXB,B,A	186.5	4464.0	B4
1A 1744-361	267.057	-36.130	1.3	0.7±0.1	0.9±0.1	LMXB,B,T	23.1	3110.0	S181B3
IGR J17487-3124	267.172	-31.382	3.0	0.6±0.1	1.1±0.1	?	8.8	5031.0	B5
IGR J17488-3253	267.217	-32.926	1.2	2.0±0.1	2.6±0.1	AGN,Sy1	24.9	4700.0	B5
4U 1745-203	267.222	-20.368	1.4	0.6±0.1	0.9±0.2	LMXB,G,T	20.7	3496.0	R120B1
AX J1749.1-2733	267.273	-27.554	1.5	1.5±0.1	1.5±0.1	HMXB?,SFXT?	19.7	4030.0	R110B1
SLX 1746-331	267.457	-33.200	1.0	1.5±0.1	2.5±0.1	LMXB,BHC,T	31.4	4631.0	S100B3
4U 1746-37	267.550	-37.048	0.8	3.8±0.1	< 0.3	LMXB,G,B,A	39.9	2867.0	B4
IGR J17507-2647	267.677	-26.792	2.6	0.9±0.1	0.9±0.1	?	10.4	4563.0	B5
IGR J17507-2856	267.681	-28.941	2.2	0.5±0.1	0.3±0.1	?,T	12.3	5153.0	S227B3
GRS 1747-312	267.684	-31.311	1.7	1.3±0.1	1.0±0.1	LMXB,G,T	16.2	4993.0	B4
IGR J17513-2011	267.823	-20.204	1.7	1.5±0.1	1.7±0.2	AGN,Sy1.9	16.2	3628.0	B3
IGR J17515-1533	267.882	-15.544	4.8	0.3±0.1	< 0.4	?	5.2	2029.0	R423B1
SWIFT J1753.5-0127	268.371	-1.456	0.7	5.2±0.2	6.9±0.4	LMXB,BHC,T	46.0	620.0	R365B1
IGR J17544-2619	268.586	-26.324	1.6	1.0±0.1	0.3±0.1	HMXB,SFXT	18.2	5009.0	R113B2
IGR J17586-2129	269.657	-21.327	3.3	0.6±0.1	< 0.3	?	7.7	4028.0	B5
IGR J17597-2201	269.935	-22.026	0.6	6.2±0.1	5.4±0.1	LMXB,B,D	66.7	3832.0	B5
GX 5-1	270.283	-25.081	0.2	56.0±0.1	3.5±0.1	LMXB,Z	889.3	4417.0	B4

TABLE 1
3RD IBIS/ISGRI CATALOG

GRS 1758-258	270.303	-25.746	0.2	58.8±0.1	75.3±0.1	LMXB,BHC	812.7	4708.0	B3
GX 9+1	270.389	-20.531	0.3	18.3±0.1	0.4±0.2	LMXB,A	275.2	3445.0	B4
SAX J1802.7-2017	270.661	-20.304	0.7	6.0±0.1	1.8±0.2	HMXB,XP,T	53.3	3469.0	B1
IGR J18027-1455	270.685	-14.916	1.5	2.5±0.1	2.6±0.2	AGN,Sy1	18.7	2024.0	B5
IGR J18048-1455	271.197	-14.966	3.4	1.0±0.1	0.5±0.2	HMXB	7.5	2046.0	B4
XTE J1807-294	271.748	-29.409	1.1	0.8±0.1	0.8±0.1	LMXB,msecXP,T	28.1	4446.0	R046B1
SGR 1806-20	272.154	-20.413	0.8	3.6±0.1	4.5±0.2	SGR	38.9	3450.0	B3
PSR J1811-1926	272.827	-19.417	2.9	0.8±0.1	1.0±0.2	PSR,SNR,PWN?	9.0	3531.0	B3
IGR J18134-1636	273.350	-16.598	3.8	0.7±0.1	1.0±0.2	?	6.7	2643.0	B5
IGR J18135-1751	273.395	-17.871	2.2	1.1±0.1	1.7±0.2	SNR,PWN?	12.2	3009.0	B3
GX 13+1	273.628	-17.158	0.3	13.8±0.1	2.4±0.2	LMXB,B,A	151.3	2668.0	B4
1M 1812-121	273.775	-12.099	0.3	26.7±0.1	26.6±0.2	LMXB,B	198.3	1694.0	B5
GX 17+2	274.007	-14.036	0.2	71.0±0.1	3.8±0.2	LMXB,B,Z	671.8	1880.0	B4
IGR J18173-2509	274.328	-25.151	2.2	1.5±0.1	0.5±0.1	?	12.3	3583.0	B5
XTE J1817-330	274.431	-33.025	0.3	6.9±0.1	4.2±0.2	XB,BHC,T	161.7	3637.0	R408B1
SAX J1818.6-1703	274.657	-17.045	0.9	1.6±0.1	1.3±0.2	HMXB,SFXT	34.3	2495.0	R110B1
AX J1820.5-1434	275.126	-14.568	1.1	2.8±0.1	1.8±0.2	HMXB,XP,Be	27.6	1869.0	S047B1
IGR J18214-1318	275.335	-13.330	2.3	1.7±0.1	1.7±0.2	?,T	11.6	1718.0	B5
4U 1820-303	275.917	-30.362	0.2	35.6±0.1	2.0±0.2	LMXB,G,B,A	442.4	3430.0	B4
IGR J18244-5622	276.062	-56.363	5.0	1.7±0.4	< 1.3	AGN,Sy2	4.9	247.0	B5
IGR J18249-3243	276.148	-32.701	4.2	0.6±0.1	0.8±0.2	AGN	6.0	2887.0	B2
IGR J18246-1425	276.161	-14.418	4.4	1.1±0.1	0.6±0.2	?	5.7	1890.0	R308B1
4U 1822-000	276.351	-0.013	1.4	2.0±0.2	< 0.5	LMXB	20.3	1433.0	B4
IGR J18256-1035	276.437	-10.563	3.7	1.0±0.1	< 0.5	?	6.8	1711.0	B1
3A 1822-371	276.449	-37.108	0.3	34.1±0.1	3.9±0.2	LMXB,D	254.5	2477.0	B4
IGR J18259-0706	276.495	-7.136	3.2	1.0±0.1	0.9±0.2	AGN?	8.1	1570.0	B5
RX J1826.2-1450	276.523	-14.833	3.2	1.0±0.1	1.7±0.2	HMXB,microQSO	8.0	2014.0	B3
Ginga 1826-24	277.371	-23.793	0.2	86.8±0.1	69.1±0.2	LMXB,B	801.7	3252.0	B5
AX J183039-1002	277.666	-10.007	4.8	0.8±0.1	< 0.5	?	5.2	1677.0	B1
IGR J18308-1232	277.696	-12.532	3.3	0.8±0.1	1.0±0.2	?	7.7	1784.0	B5
IGR J18325-0756	278.117	-7.946	1.3	2.5±0.1	1.4±0.2	?,T	21.8	1660.0	S047B1
SNR 021.5-00.9	278.388	-10.579	1.2	3.3±0.1	3.3±0.2	SNR,PWN	24.7	1692.0	B5
PKS 1830-211	278.419	-21.073	1.2	2.6±0.1	3.4±0.2	AGN,QSO	24.4	2611.0	B3
3C382	278.786	32.707	4.4	3.4±1.4	4.9±1.8	AGN,Sy1	5.6	34.0	R022B1
XB 1832-330	278.929	-32.986	0.5	10.9±0.1	10.5±0.2	LMXB,G,B,T	92.1	2576.0	B5
AX J1838.0-0655	279.509	-6.916	1.5	1.9±0.1	3.0±0.2	SNR,PWN?	18.6	1667.0	B3
ESO 103-35	279.563	-65.450	3.9	5.3±0.9	4.7±1.5	AGN,Sy2	6.5	44.0	B5
Ser X-1	279.992	5.036	0.4	11.8±0.1	0.6±0.2	LMXB,B	121.0	1750.0	B4
AX J1841.0-0535	280.243	-5.580	2.9	1.1±0.1	0.7±0.2	HMXB,XP,Be?,SFXT	9.0	1702.0	R429B2
Kes 73	280.338	-4.948	1.3	2.2±0.1	4.2±0.2	SNR,AXP	23.4	1777.0	B3
3C 390.3	280.586	79.781	2.2	2.9±0.3	4.1±0.5	AGN,Sy1	12.6	306.0	B5
IGR J18450-0435	281.259	-4.567	2.3	1.6±0.1	1.2±0.2	HMXB,SFXT	11.7	1784.0	B5
Ginga 1843+009	281.404	0.865	0.6	5.0±0.1	3.7±0.2	HMXB,XP,Be,T	55.5	1910.0	S308B3
AX J1846.4-0258	281.596	-2.983	1.8	1.7±0.1	2.4±0.2	SNR,PWN,AXP	15.6	1795.0	B3
IGR J18483-0311	282.068	-3.171	0.8	4.7±0.1	2.6±0.2	?	42.7	1802.0	R429B1
3A 1845-024	282.076	-2.425	2.3	0.7±0.1	0.6±0.2	HMXB,XP,Be,T	11.4	1753.0	R231B1
IGR J18485-0047	282.115	-0.779	3.4	1.0±0.1	0.8±0.2	?	7.6	1858.0	B5
IGR J18490-0000	282.278	-0.017	3.0	1.1±0.1	1.2±0.2	?	8.6	1949.0	B5
4U 1850-087	283.264	-8.704	0.9	5.2±0.1	4.4±0.2	LMXB,G,B	38.3	1517.0	B5
IGR J18539+0727	283.490	7.469	1.1	0.8±0.1	1.2±0.2	XB,BHC,T	27.8	2284.0	R062B1
V1223 Sgr	283.755	-31.154	0.8	7.4±0.2	3.0±0.3	CV,IP	41.3	1371.0	B1
XTE J1855-026	283.878	-2.608	0.5	12.2±0.1	7.2±0.2	HMXB,XP,T	91.0	1821.0	B5
2E 1853.7+1534	283.970	15.618	2.4	1.5±0.2	1.4±0.2	AGN,Sy1	11.2	1405.0	B5
XTE J1858+034	284.678	3.439	0.3	13.9±0.1	1.7±0.2	HMXB,XP,Be,T	213.5	2419.0	R189B2
HETE J1900.1-2455	285.035	-24.924	0.6	6.6±0.2	5.6±0.3	LMXB,msecXP,B	56.1	1013.0	S411B3
XTE J1901+014	285.417	1.448	1.1	3.0±0.1	2.8±0.2	XB,BHC?,T	27.4	2248.0	B5
4U 1901+03	285.915	3.203	0.2	37.7±0.1	4.5±0.2	HMXB,XP,T	478.3	2483.0	S047B1
IGR J19048-1240	286.205	-12.661	4.2	0.6±0.2	< 0.6	?	5.9	998.0	R365B1
SGR 1900+14	286.851	9.311	2.1	1.3±0.1	1.1±0.2	SGR	13.3	2478.0	B5
XTE J1908+094	287.225	9.384	0.9	1.7±0.1	1.9±0.2	LMXB,BHC,T	35.6	2471.0	S047B3
4U 1907+097	287.411	9.830	0.3	18.6±0.1	1.9±0.2	HMXB,XP,T	179.3	2431.0	B4
AXJ1910.7+0917	287.664	9.273	3.4	0.7±0.1	0.6±0.2	?	7.5	2517.0	B5
4U 1909+07	287.701	7.596	0.4	14.9±0.1	8.6±0.2	HMXB,XP	137.6	2560.0	B5
Aql X-1	287.814	0.585	0.4	13.6±0.1	11.9±0.2	LMXB,B,A,T	133.7	1942.0	S308B3
SS 433	287.956	4.983	0.5	10.4±0.1	5.2±0.2	HMXB,SG,microQSO	94.7	2560.0	B5
IGR J19140+0951	288.516	9.878	0.5	8.9±0.1	5.6±0.2	HMXB,SG	81.5	2339.0	B5
GRS 1915+105	288.799	10.944	0.2	296.8±0.1	123.4±0.2	LMXB,BH,T	2556.6	2342.0	B4
4U 1916-053	289.701	-5.238	0.6	9.9±0.2	5.4±0.3	LMXB,B,D	58.8	1147.0	B5
SWIFT J1922.7-1716	290.633	-17.305	3.8	1.0±0.3	< 0.9	?	6.7	474.0	S308B3
1RXS J192450.8-291437	291.246	-29.235	5.0	1.1±0.3	1.2±0.4	AGN,BL Lac	5.0	506.0	B3
IGR J19267+1325	291.670	13.425	3.7	0.7±0.1	0.6±0.2	?	6.8	1792.0	B5
IGR J19378-0617	294.413	-6.218	4.4	1.5±0.2	< 0.8	AGN,Sy1	5.7	601.0	B5
RX J1940.1-1025	295.058	-10.428	3.0	2.7±0.3	2.0±0.5	CV,P,asynch	8.7	369.0	B1
IGR J19405-3016	295.120	-30.266	5.4	0.9±0.3	1.2±0.5	AGN	4.6	371.0	B1
NGC 6814	295.657	-10.320	2.4	3.2±0.3	3.7±0.6	AGN,Sy1.5	11.4	329.0	B5
IGR J19443+2117	296.069	21.287	4.9	1.4±0.3	0.9±0.4	?	5.1	574.0	B3
IGR J19473+4452	296.823	44.906	4.5	1.8±0.3	1.8±0.4	AGN,Sy2	5.6	467.0	B3

TABLE 1
3RD IBIS/ISGRI CATALOG

IGR J19487+5120	297.184	51.336	4.4	< 0.9	< 1.3	?	5.7	240.0	R323B2
KS 1947+300	297.395	30.209	0.8	13.5±0.3	9.7±0.4	HMXB,XP,T	43.3	502.0	B5
4U 1954+31	298.926	32.102	1.2	7.0±0.2	3.0±0.3	LMXB,NS?	25.0	677.0	B1
Cyg X-1	299.590	35.199	0.2	763.7±0.2	876.7±0.3	HMXB,BH,U	4651.3	1142.0	B5
Cyg A	299.868	40.749	1.4	4.8±0.2	4.8±0.3	AGN,Sy2	20.1	789.0	B5
SWIFT J2000.6+3210	300.085	32.177	2.9	2.0±0.2	1.8±0.3	HMXB,Be	8.9	734.0	B5
ESO 399-20	301.691	-34.559	4.9	1.7±0.4	1.4±0.7	AGN,Sy1	5.1	241.0	B5
IGR J20186+4043	304.690	40.703	3.3	1.3±0.2	1.3±0.3	AGN?	7.8	954.0	B5
IGR J20286+2544	307.135	25.772	4.4	2.6±0.5	3.8±0.6	AGN,Sy2	5.7	230.0	B3
EXO 2030+375	308.059	37.638	0.3	32.4±0.2	16.3±0.3	HMXB,XP,Be,T	150.0	1009.0	B5
Cyg X-3	308.108	40.956	0.2	196.5±0.2	78.3±0.3	HMXB	1096.2	1000.0	B4
4C 74.26	310.585	75.145	3.9	3.2±0.5	2.6±0.9	AGN,QSO	6.4	113.0	B5
SAX J2103.5+4545	315.894	45.749	0.5	16.0±0.2	7.8±0.3	HMXB,XP,Be,T	87.2	988.0	B5
S52116+81	318.492	82.072	3.5	2.5±0.4	2.3±0.7	AGN,Sy1	7.3	199.0	B5
IGR J21178+5139	319.436	51.663	4.0	1.2±0.2	1.4±0.3	AGN?	6.2	685.0	B3
V2069 Cyg	320.906	42.278	4.9	0.9±0.2	< 0.5	CV,IP	5.1	901.0	B4
IGR J21247+5058	321.172	50.972	1.0	6.0±0.2	6.7±0.3	AGN,Sy1	31.7	768.0	B5
IGR J21272+4241	321.792	42.692	5.5	0.9±0.2	< 0.5	?	4.5	791.0	B1
SWIFT J2127.4+5654	321.866	56.918	3.6	2.3±0.3	< 1.0	AGN,NL Sy1	7.0	348.0	B1
IGR J21335+5105	323.438	51.121	1.6	3.8±0.2	1.6±0.3	CV,IP	17.8	710.0	B5
IGR J21347+4737^s	323.673	47.620	4.5	1.1±0.2	0.7±0.3	?	5.6	845.0	B5
RX J2135.9+4728^t	324.016	47.535	4.7	1.0±0.2	0.9±0.3	AGN,Sy1	5.3	843.0	B1
SS Cyg	325.691	43.583	1.6	3.8±0.2	1.6±0.3	CV,DN	17.8	745.0	B4
Cyg X-2	326.169	38.320	0.3	28.5±0.2	2.9±0.3	LMXB,B,Z	202.1	730.0	B4
NGC 7172	330.492	-31.874	1.7	4.8±0.3	4.9±0.6	AGN,Sy2	17.0	271.0	B5
BL Lac	330.678	42.288	3.8	1.4±0.2	1.7±0.4	AGN,BL Lac	6.8	544.0	B5
4U 2206+543	331.987	54.508	1.0	8.0±0.3	5.7±0.4	HMXB,Be	31.4	531.0	B5
FO Aqr	334.478	-8.317	5.1	3.6±0.7	< 2.8	CV,IP	4.8	84.0	B1
IGR J22234-4116	335.850	-41.262	5.3	< 0.9	3.2±0.9	?	4.6	146.0	B2
IGR J22292+6647	337.295	66.788	4.8	0.9±0.2	0.6±0.3	AGN,RG	5.1	988.0	B1
NGC 7314	338.932	-26.076	4.9	2.3±0.5	2.2±0.9	AGN,Sy1.9	5.1	164.0	B5
MR 2251-178	343.543	-17.607	3.5	3.4±0.6	5.0±1.1	AGN,Sy1	7.3	101.0	B5
MCG-02-58-022	346.200	-8.666	3.7	2.8±0.4	1.9±0.8	AGN,Sy1.5	6.9	147.0	B1
IGR J23130+8608	348.261	86.133	4.8	1.9±0.5	< 1.8	?	5.2	134.0	B5
NGC 7603	349.692	0.206	5.5	2.6±0.6	< 2.2	AGN,Sy1.5	4.5	87.0	B1
Cas A	350.848	58.815	0.9	4.1±0.1	2.4±0.2	SNR	34.2	1633.0	B4
IGR J23308+7120	352.694	71.336	4.5	0.9±0.2	< 0.6	AGN?	5.5	982.0	B1
IGR J23524+5842	358.111	58.700	4.0	0.7±0.1	0.8±0.2	?	6.3	1789.0	B5

^a Names in bold face indicate new detections since second catalog

^b Position errors expressed as radius of 90% confidence circle in arcminutes

^c Time-averaged flux expressed in units of mCrab; appropriate conversion factors are: (20-40 keV) 10 mCrab = 7.57×10^{-11} erg cm⁻² s⁻¹ = 1.71×10^{-3} ph cm⁻² s⁻¹; (40-100 keV) 10 mCrab = 9.42×10^{-11} erg cm⁻² s⁻¹ = 9.67×10^{-4} ph cm⁻¹ s⁻¹

^d Source type classifications: A=Atoll source (neutron star); AGN=Active galactic nuclei; AXP=Anomalous X-ray pulsar; B=Burster (neutron star); Be=B-type emission-line star; BH=Black hole (confirmed mass evaluation); BHC=Black hole candidate; Cluster=Cluster of galaxies; CV=Cataclysmic variable; D=Dipping source; DN=Dwarf Nova; G=Globular Cluster X-ray source; GRB=Gamma-Ray Burst; HMXB=High-mass X-ray binary; IP=Intermediate Polar; LMXB=Low-mass X-ray binary; Mol Cloud=Molecular cloud; NS=Neutron Star; P=Polar; PSR=Radio pulsar; PWN=Pulsar wind nebula; QSO = Quasar; RG=Radio Galaxy; SFXT=Supergiant Fast X-ray Transient; SG=Supergiant; SGR=Soft gamma-ray repeater; SNR=Supernova remnant; Sy=Seyfert galaxy; Symb=Symbiotic star; T=Transient source; U=Ultrasoft source; XB=Galactic X-ray binary; XP=X-ray pulsar; Z=Z-type source (neutron star)

^e Maximum significance in a single map; see mapcode column to identify map with maximum significance

^f Corrected on-source exposure (ksec)

^g Map with maximum significance: B1=20-40 keV, B2=30-60 keV, B3=20-100 keV, B4=17-30 keV, B5=18-60 keV; a prefix of RXXX indicates detection in revolution XXX, SXXX indicates detection in revolution sequence beginning at revolution XXX; ST = Staring data

^h Source type from Veron and Veron

ⁱ Possibly associated with BAL QSO, SDSS J03184-0015

^j Possibly blended with ESO121-28, 4.8' away

^k Eta Carinae or source therein

^l Source type from CFA catalogue

^m Significantly offset from original source position

ⁿ Blended with NGC 6221

^o Blended with ESO 138-1

^p Coincident with Sgr A*, but not unambiguously identified; in confused Galactic Center region

^q Coincident with G0.13-0.13 molecular cloud; in confused Galactic Center region

^r In confused Galactic Center region

^s Blended with RX J2135.9+4728

^t Blended with IGR J21347+4737